PERIODICO di MINERALOGIA
established in 1930

Dipartimento di Scienze della Terra
Sapienza Università di Roma

An International Journal of
Mineralogy, Crystallography, Geochemistry,
Ore Deposits, Petrology, Volcanology
and applied topics on Environment, Archaeometry and Cultural Heritage

Cytotoxicity *in vitro* of two non-commercial samples of chrysotile and fibrous erionite

Armanda Pugnaloni [1,*], Silvia Di Valerio [1], Giovanni Tossetta [2], Tatiana Armeni [3], Laura Cianfruglia [3], Luca Tiano [3], Fabio Marchegiani [3], Stipa Pierluigi [4], Emiliano Laudadio [4], Simona Sabbatini [4], Cristina Minnelli [4], Salvatore Vaiasicca [1], Deborah Ramini [5], Antonio D. Procopio [1], Francesca Fazioli [1], Alessandro F. Gualtieri [6]

[1] Department of Clinical and Molecular Sciences, Polytechnic University of Marche, Via Tronto 10/a, I-60126 Torrette di Ancona, Italy
[2] Department of Experimental and Clinical Medicine, Polytechnic University of Marche, Via Tronto 10/a, I-60126 Torrette di Ancona, Italy
[3] Department of Life and Environmental Sciences, Polytechnic University of Marche, Via Brecce Bianche, I-60131 Ancona, Italy
[4] Department of Science and Engineering of Materials, Environment and Urban Planning, Chemistry division, Polytechnic University of Marche, Via Brecce Bianche, I-60131 Ancona, Italy
[5] Clinic of Laboratory and Precision Medicine, IRCCS INRCA, via Birrarelli 8, 60121 Ancona, Italy
[6] Department of Chemical and Geological Sciences, University of Modena and Reggio Emilia, Via G. Campi 103, I-41125 Modena, Italy

ARTICLE INFO

Submitted: February 2023
Accepted: July 2023
Available on line: August 2023

* Corresponding author:
armanda.pugnaloni@staff.univpm.it

Doi: 10.13133/2239-1002/18017

How to cite this article:
Pugnaloni A. et al. (2023)
Period. Mineral. 92, 241-259

ABSTRACT

Exposure to naturally occurring asbestos and fibrous erionite can have severe impacts for the human health and cause malignant mesothelioma. The disease burden associated with this exposure is difficult to quantify and is not properly investigated. A characterization of the crystal-chemical-physical properties and toxicity/carcinogenicity of naturally occurring fibres with attention to asbestos and erionite is therefore highly recommended. The present study deals with the *in vitro* biological effects in MeT5A and A549 human cell lines of two non-commercial asbestos fibres: Valmalenco chrysotile from Central Alps Italy and fibrous erionite from Jersey Nevada, USA, including the standards UICC Chrysotile and UICC crocidolite.

Light and scanning electron microscopy (SEM) observations showed morphological cell perturbation of treated cells. SEM-EDAX investigations revealed that the release of chemical components in the culture media affect cell viability. ROS levels increased in accordance with glutathione depletion, witnessing a remarkable cellular stress. Free radical release on pristine fibres was investigated by means of electron paramagnetic resonance (EPR) spin trapping technique and FTIR spectroscopy to characterize the molecular structures of fibres.

Results reflect the cytotoxic effects and evidence the different toxicity pathways prompted by these fibre species due to their different crystal assemblages and physical properties.

Keywords: asbestos; environmental exposure; chrysotile; erionite; cytotoxicity.

BACKGROUND

Asbestos is a generic term used to describe six mineral species that belong to the silicate families of serpentine and amphiboles. The serpentine family contains only chrysotile (commonly known as white asbestos) which accounts for some 90-95% of all asbestos that was and still used worldwide; amphibole category includes asbestos actinolite, amosite (brown asbestos), asbestos

anthophyllite, crocidolite (blue asbestos) and asbestos tremolite (Gualtieri, 2023). Despite generally grouped as asbestos, these minerals have different geological occurrences and significant differences in crystalline structures and chemical compositions (Sporn, 2011). Asbestos is known to represent a severe hazard for human health, being listed as the third most abundant pollutant on a global scale (Takahashi et al., 2016; Furuya et al., 2018). Internalization of respirable micro- to nano-sized asbestos fibres can lead to their gradual accumulation, particularly in the deep respiratory system (Whysner et al., 1994; Bernstein, 2014), where they drive different pathogenic effects such as chronic inflammation, asbestosis, pleural effusion, and, as later manifestations, malignancies such as lung carcinoma or pleural mesothelioma (Klebe et al., 2019). Asbestos-related diseases (ARDs) are well known as occupational pathologies; however, in recent year, health hazards resulting from environmental exposure have been reported even at low doses, not only with regard to regulated asbestos fibres (Dumortiet et al., 2002) but also to non-regulated mineral fibres (generally known as asbestiform minerals) (Comba et al., 2005).

Although there has been a substantial reduction in the global use of asbestos in the last 50 years and a progressive ban in many developed countries, hazardous mineral fibres are still present in the life environment such as public or private buildings, abandoned industrial sites or in the natural environment (the so-called naturally occurring asbestos or NOA) and especially in soils and in close proximity to former asbestos mines or quarries. It should be also noted that people can be exposed to asbestos contaminated waters as asbestos fibres can be eroded by natural deposits or by asbestos deposits in landfills, by the asbestos pipes that are used to transport drinking water or by filters containing asbestos (Totaro et al., 2019).

In addition to the asbestos minerals, there are other fibrous/asbestiform minerals known to represent a health hazard and classified as carcinogenic agents (see for example, fibrous fluoroedenite: Gianfagna et al., 2003). Among them, the zeolite erionite is certainly the most relevant and investigated non-asbestos mineral fibre to date. Zeolites are composed of three-dimensional framework of tetrahedra usually centred by Si and Al, where all the vertices of the tetrahedra are shared with other tetrahedra and show peculiar chemical-physical properties such as ion exchange. Owing to a relevant chemical variability, three different species, erionite-K, erionite-Ca and erionite-Na have been recognized to date (Ballirano and Cametti, 2015). Erionite generally displays a fibrous and or asbestiform crystal shape. It is formed as diagenetic alteration product of sediments, in cavities of altered basalts or as a hydrothermal alteration product (Ballirano et al., 2017). Erionite of diagenetic origin is responsible for an unprecedented epidemic of malignant mesothelioma that has struck three villages, Karain, Tuzkoy and Sarihidir, in Cappadocia, Turkey (Carbone et al., 2007).

Although the epidemiological association between asbestos exposure and fibrotic and malignant lung diseases is well established, the mechanisms linking asbestos exposure to the development of ARDs are still subject of deep scrutiny (Gualtieri, 2023). According to Srivastava et al. (2010), the asbestos fibres toxicology has been associated with dose, dimension, durability and chemical composition. Regarding this last aspect, the role of several elements such as Al, Fe, Mn, Mg, Ca, Si, Zn and Na released from asbestos fibres is still a subject of intensive multidisciplinary investigations (Srivastava et al., 2010; Mossman et al., 2011). A systematic chemical-physical, mineralogical and structural characterization of the fibres was supported since 2017 by the long term Italian Research Project of National Interest (PRIN). The project focuses on the chemical content and environment effect in mineral fibres and their surface reactivity since they play a crucial role in ARDs (Bloise et al., 2016; Franzblau et al., 2020). Among the diseases promoted by asbestos, malignant mesothelioma is considered a marker of asbestos exposure (Jarvholm and Astrom, 2014). According to Thompson et al. (2014), asbestos exposure is correlated to an imbalance of reactive oxygen species (ROS) and depletion of antioxidants like glutathione, an important non-enzymatic antioxidant agent that responds to cellular stress.

In this study, we have compared the *in vitro* biological effects of two natural non-commercial mineral fibres that can eventually cause environmental exposure: chrysotile from Valmalenco and fibrous erionite-Na from Jersey (Nevada, USA). The human mesothelial virus transformed cells line (MeT5A) and alveolar epithelial cells from human adenocarcinoma (A549) were used for the *in vitro* viability tests, and ROS production and depletion of intracellular glutathione. For comparison, well characterized standard asbestos fibres such as UICC chrysotile and UICC crocidolite were also tested. Interaction of the cells with the fibres on a morphological standpoint was observed by Scanning Electron Microscopy (SEM). In addition, SEM-EDAX microanalysis was performed to qualitatively assess the chemical composition of the fibres with particular attention to the elements released in the culture media by the fibres.

With the aim to clarify the relationship between Fe ions surface occurrence and asbestos reactivity, free radical release was investigated by means of electron paramagnetic resonance (EPR) spin trapping technique (Janzen and Blackburn, 1968; Chalfont et al., 1968; Lagercrantz and Forshult, 1968) considering the Fenton reaction, which is one of the most biologically relevant

reactions known to occur *in vivo* between H_2O_2 and Fe (II) ions present in asbestos surface, producing hydroxyl radicals ($HO^{\bullet}$) rapidly trapped by 5,5-dimethyl-3,4-dihydro-2H-pyrrole N-oxide (DMPO), which likely represents the most used water-soluble Spin Trap (Buettner, 1987; Fubini et al., 1995; Bode et al., 2020; Stipa, 2021). FTIR spectroscopy is frequently used for the characterization and identification of asbestiform minerals. Vibrational spectra can be collected either on powders or on single crystals, requiring only a very small amount of material (mg) such as tiny crystals with sizes ranging from some mg to few tens of mm. In this case, Attenuated Total Reflectance-Fourier Transform Infrared (ATR-FTIR) spectroscopy has been used in order to characterize the molecular structures of fibres.

MATERIAL AND METHODS

Preparation of the mineral fibres

Mineral fibres used in this study were: standard UICC chrysotile (Chr-UICC) with chemical formula $Mg_{2.92}(OH)_4Si_{1.96}Fe_{0.08}Al_{0.06}O_5$, chrysotile from Valmalenco (Chr-VM) with chemical formula $Mg_{2.68}(OH)_4Si_{2.06}Fe_{0.08}Al_{0.07}O_5$, standard UICC crocidolite (Cro-UICC) with formula $Na_{2.53}Fe^{3+}_{2.19}Fe^{2+}_{1.47}Mg_{0.79}Ca_{0.02}Si_{8.06}O_{22}(OH)_2$, and fibrous erionite from Jersey Nevada (Eri-JN) characterized by the chemical formula $Fe^{3+}_{0.29}(Na_{5.35}K_{2.19}Ca_{0.15}Mg_{0.11}Ti_{0.05})_{7.85}$ $[Si_{28.01}Al_{7.90}]_{35.91}O_{72})\cdot 28.13H_2O$ (Gualtieri et al., 2016).

Wollastonite fibres with a mean chemical formula of $Ca_{0.997}Fe^{2+}_{0.0053}Fe^{3+}_{0.0024}Mn_{0.0025}Si_{0.9786}O_3$ (Di Giuseppe et al., 2021b) were selected as negative control standard and administered for morphological evaluation in Light microscopy investigations and in MTT test to assay cell viability.

All fibres have been already fully characterized elsewhere (Bloise et al., 2016; Bursi Gandolfi et al., 2016; Cattaneo et al., 2012; Giordani et al., 2022; Pollastri et al., 2014, 2015, 2016; Turci et al., 2012).

The fibres were weighed, re-suspended by vortex in culture medium and added to cultures at a final concentration of 50 mg/ml, equal to 14 $\mu g/cm^2$ (Giantomassi et al., 2010).

EPR measurement of free radical production

Samples were incubated in a H_2O_2 0.1 M solution buffered at pH 7.4 for 1 h. These conditions were chosen to promote the dissolution dynamics of asbestos in a reasonable experimental time mimicking the cellular environment. To assess the surface reactivity of the investigated systems, the hydroxyl radicals ($HO^{\bullet}$) were produced by the Fenton reaction: $Fe^{2+}_{surf}+H_2O_2 \rightarrow Fe^{3+}_{surf}+OH^-+HO^{\bullet}$. In the presence of DMPO as Spin Trap, the surface-generated $HO^{\bullet}$ radicals were rapidly trapped to yield the corresponding $[DMPO\text{-}HO]^{\bullet}$ adduct characterised by its typical EPR signal. Each resulting recorded EPR spectrum was transformed by double integration to evaluate the total amount of radicals released during 1 h of incubation of the asbestos fibres.

X-band EPR measurements have been carried out on a Bruker EMX/Xenon spectrometer system equipped with a microwave frequency counter and an NMR Gauss meter for field calibration; for g-factor determination, the whole system was standardized with a sample of perylene radical cation in concentrated sulfuric acid (g-factor = 2.00258). Quantitative estimations have been performed using the native (Xenon) spectrometer software, standardized with proper alanine samples. Instrument parameters were set up as follows: Modulation Frequency: 100 kHz; Time Constant: 0.01 ms; Sweep Width: 100 G; Modulation Power: 10.52 mW; Modulation Amplitude: 1.0 G; Sweep Time: 5.24 s.

ATR-FTIR Measurements

IR spectra were collected in reflectance mode using a Perkin Elmer Spectrum GX1 spectrometer, equipped with DTGS detectors and Attenuated Total Reflectance (ATR) attachment with a zinc selenide (ZnSe) crystal. The spectral range was 4000-550 cm^{-1}, with a spectral resolution of 4 cm^{-1}; each spectrum was the result of 32 scans. Samples were directly deposited onto the ZnSe crystal without requiring any preparation. Then, five IR spectra have been acquired on each sample. The background spectrum being collected on the clean crystal under the same conditions. Raw IR spectra were converted in absorbance mode and vector normalized (Spectrum 10.4.0 software, Perkin-Elmer).

Cell cultures and managements

The Human epithelial cells lines used in this study include Mesothelium virus transformed (MeT5A) and Adenocarcinoma lung cancer (A549) purchased from ATCC® (Rockville, USA). The cells were maintained in standard culture medium represented by Roswell Park Memorial Institute (RPMI-1640) medium (Sigma-Aldrich, Milan, Italy) supplemented with 10% foetal bovine serum (FBS) (Gibco, USA), 2mM l-glutamine, 100U/ml penicillin and 100U/ml streptomycin (Sigma-Aldrich, Milan, Italy). Cells were maintained at 37 °C in a humidified atmosphere of 5% CO_2. In all experiments, the cells were exposed at three time points (6, 24 and 48 h). Untreated cultures were considered as control samples (CTRL).

Light microscopy assays

Morphological observation on MeT5Aand A549 cells by light and fluorescent microscopy for DAPI staining.

Morphological investigations were performed in

control and treated MeT5A and A549 cells at 24 h with a light inverted microscope (Nikon Eclipse T100).

For apoptosis assay, control and treated cells were washed in Dulbecco's PBS (Euroclone), fixed in 4% paraformaldehyde in PBS for 10 min at 4 °C and permeabilized in 0.1 M PBS added with 0.1% Triton X-100 (Sigma, Milano, Italy) for 5 min. After washing in PBS nuclear staining was carried out by using DAPI probe. Cells treated for 2 h with 400 μM H_2O_2 were considered as positive control. Apoptotic cells were counted in five different microscopic non-overlapped fields from each slide and expressed as mean of percent apoptotic cells (AC) ± standard deviation (sd).

Scanning electron microscope/energy dispersive X-ray spectroscopy (SEM–EDS)

Specimens were fixed in 2% (v/v) glutaraldehyde in 0.1 M sodium cacodylate buffer (pH 7.4) for 30 min at 37 °C, washed in three PBS changes, postfixed in 1% OsO4 in 0.1 M sodium cacodylate buffer for 1 h at 4◦C, dehydrated with a graded alcohol series, CPD dried and mounted to sample holders with conductive carbon rib-bon. Samples were analysed with a Zeiss Supra 40 scanning electron microscope connected to a Bruker dispersive energy spectrometer (EDS X Flash) to detect chemical composition of the mineral samples. A quantitative analysis was carried out by X-ray spectroscopy considering each element and elaborating the data by ZAF correction method. Mean values ± SD chemical content of 10 analyses were expressed as weight percent (wt%).

Cell viability test (MTT assay)

MTT (3(4,5dimethylthiazol2yl) 2,5diphenyltetrazolium bromide) (Sigma-Aldrich) test was performed to evaluate cytotoxic effects of the different fibres. The MTT test consist in a colorimetric assay (Lanone et al., 2009) which measures the conversion of MTT to insoluble formazan by dehydrogenase enzymes of the intact mitochondria of living cells. MeT5A and A549 cells were seeded at the density of 2.0×10^4 cells/cm^2 for MeT5A and 1.0×10^4 cells/cm^2 for A549 in 24 well/plate, left adhere for 24 h, and then treated with fibres suspension. For each time point the medium was removed, 500 μl of RPMI with 50 μl of MTT solution (5 mg/ml) were added and incubated for 4 h at 37 °C. At the end of incubation, the medium was removed and the formazan crystals dissolved in 400 μl of dimethyl sulfoxide (DMSO) (Sigma-Aldrich, Milan, Italy). The quantity of crystals formed is correlated directly with the viable cells. Optical density (OD) was measured at 540 nm using a spectrophotometer (Neo Biotech NB-12-0035). Untreated cells were used as controls and their absorbance values taken as reference. Results were expressed as mean ± standard deviation (SD) of % values of viable cells.

Trypan Blue Exclusion Assay

Trypan blue is a diazo dye which is actively excluded by viable cells, but is taken up by dead cells, so that at microscopy observation live and dead cells appear unstained and blue stained respectively. In our study, the number of viable cells present in a cell suspension after treatments with asbestos fibres was investigated by trypan blue exclusion. Briefly, the cells after all treatments were washed, trypsinized and centrifuged at 500 g for 5 min. The pellets were then re-suspended in 1 ml of medium and an aliquot of 10ml was mixed 1:1 with 0.4% solution of trypan blue in buffered solution, pH 7.3. 10 μl of solution was observed and counted in a Burker camera by light microscopy (Nikon Eclipse T100). The percentage of dead cells per ml was obtained by the following formula:

$$\text{Dead cells \%} = \frac{\text{Total number of dead cells per ml}}{\text{Total numer of cells per ml}} x\ 100$$

With this method the number of viable cells reflects cell proliferation (increases) or cytotoxicity (decreases) in comparison to control, untreated cells.

Reactive Oxygen Species (ROS)

Cellular oxidative stress induced by asbestos fibres treatments was measured using the fluorescent probe, H2DCFDA (Carboxy-H2DCFDA-C400, Invitrogen).

The H2DCFDA crossing the plasma membrane of the cell, is de-acetylated to H2DCF producing a fluorescent product, DCF. MeT5A and A549 cells (1.5×10^4 and 1.0×10^4 cells/cm^2 respectively in 12-well plates) were cultured for 24 hours in RPMI-1640 before treatment with asbestos fibres for 6, 24 and 48 h in the same culture medium. At the end of each time points cells were trypsinized, centrifuged at 600 x g for 5 min, washed twice with PBS and incubated for 30 min in the dark at 37 °C in PBS containing 10 μM (work solution) of Carboxy-H2DCFDA (1mM) probe for 30 min at 37 °C in the dark. After the incubation the reaction was stopped with 1ml of filtered PBS followed by centrifuged at 500 g for 7 min. The supernatant was then removed and the cells resuspended in 200 μl of filtered PBS. The cells were stained with 4 μl of Propidium Iodide (PI) 10μg/ml to exclude dead cells from the counts. Fluorescence intensity was measured using flow cytometry (Guava® easy Cyte™ Flow Cytometer; Millipore) with excitation at 488 nm. Emissions were recorded using the green channel for Carboxy-H2DCFDA and the red channel for the PI. Mean Fluorescence Intensity (MFI) was recorded on an average of 10,000 events from each sample. Experiments were carried out at least in triplicates and results were analysed by FlowJo software. Results

were expressed as mean values ± standard deviation (sd) of fluorescence intensity.

Cellular Glutathione

Total glutathione was measured spectrophotometrically at 412 nm using the glutathione reductase (GR) recycling assay in the presence of 5,5-dithiobis (2-nitrobenzoic acid) (DTNB), with a calibration curve obtained with known concentrations of GSH (Brigelius et al., 1983). Briefly, cells were trypsinized, washed twice in cold PBS, and de-proteinized in 1% sulfosalicylic acid for 30 min at 4 °C. After centrifugation, the supernatant was recovered and analysed for glutathione quantification. The pellet was re-suspended with 1 M NaOH for recovery and quantification of proteins by Bradford methods using BSA as standard. The level of intracellular total glutathione was expressed as nmol/mg protein (Damiani et al., 2018).

Statistical analysis

Statistical analysis was performed using Prisma 8 for Windows (Prisma Software). Three biological independent replicates for each experiment (DAPI staining, SEM, MTT, ROS and Glutathione) were performed. Results were reported as mean ± standard deviation (SD). Unpaired t test analysis was used to assess differences among groups.

RESULTS AND DISCUSSION

Morphological and ultrastructural analysis of fibres-treated cultures

Light microscopy investigations of MeT5A (Figure 1a) and A549 (Figure 1b) cells. Untreated cultures showed aspects of semi-confluent cultures with normal morphology of healthy cells in state of adhesion and migration in the attempt to crowd the culture. Cell cultures treated for 48 h with 50 μg/ml of fibres (↑) showed signs of structural perturbations such as cell vacuolization and necrosis, according to the different degrees of cell damage exerted by the fibres. After wollastonite contacts cells showed better morphology.

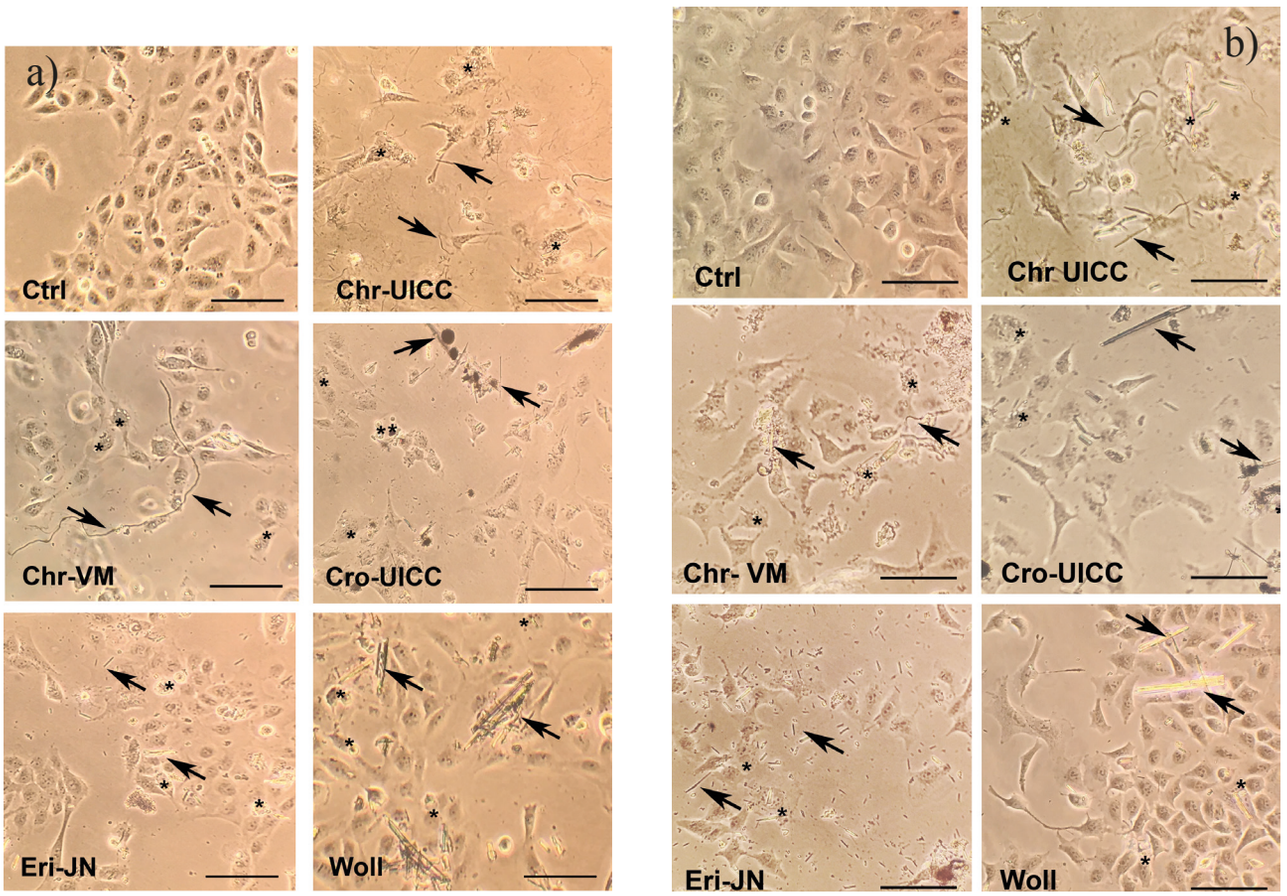

Figure 1 a,b. Light microscopy images of MeT5A (A) and A549 (B) cells at 24 h. In both experiments control cultures show morphology of healthy untreated cells. Cultures exposed for 24 h to Chr-UICC, Chr-VM, Cro-UICC, Eri-JN and Wollastonite fibres shows morphological sights of structural perturbation and vacuolation (*) due to fibres (↑) interaction in both cell lines. Wollastonite treated cultures showed less morphological perturbation after fibres contact. Scale bars = 25 μm.

Fluorescent microscopy images after DAPI staining (Figure 2 a,b) showed normal nuclei in control cells and apoptotic bodies (*) and micronuclei (↑), detectable as smaller and irregular nuclei. These findings can be considered as signs of the apoptotic cell death pathway undertaken by the cell because of nuclear DNA damage. Morphometrical investigations (Figure 2c) evidenced higher number of apoptotic cells after Chrysotile UICC and Valmalenco fibres' contact.

SEM images (Figure 3 a-c) taken using secondary electrons showed specific morphological aspects of raw asbestos fibres (Figure 3a) and fibres in Met5A and A459 culture environment (Figure 3 b,c), respectively. Fibres in the cell culture display close contacts with cell surface engaged in attempt of asbestos uptake (Fiure 3d). Fibres uptake after Eri-JN treatment was more evident due to the smaller size of the fibres.

EDAX signals recorded at 30 kv work tension are influenced by the substrate composition because. Signal depth is therefore proportional to the work tension. Qualitatively, SEM-EDAX chemical analysis on fibres in both cell cultures after 48 h treatment showed differences in comparison to the pristine fibres in element content expressed as weight % (Table 2). Keeping in mind that the comparison are qualitative, it is possible to observe that the general variations of Si and Al in the fibres after 48h of cell culture treatment are probably correlated to the presence of the same elements in the support glass, leading to additive signal detected by the electron beam. A significant trend of decrease of Mg and Fe content was detected in Chr-UICC and Chr-VM fibres in cultures with respect to the pristine cases, as these elements are released in the culture environment likely due to the partial early dissolution of the octahedral sheet of the chrysotile fibres (Gualtieri et al., 2019). Cro-UICC and Eri-JN also apparently show a minor trend of decrease of Mg.

Cell toxicity induced by mineral fibres was recently considered as consequence of their physical-chemical properties (Mossman et al., 2011; Baumann et al., 2015; Carbone and Yang, 2017). Indeed, some elements, such as Si, Al Mg and Fe interfere with cell metabolism. Chemical composition and surface properties are key features potentially related to attract iron from the surrounding environment, a phenomenon that seem to be essential in the formation of asbestos bodies in the lung, considered hallmarks of asbestos exposure (Ghio et al., 2004). It has also been reported that *in vivo* Mg contributes with iron in the first steps of interaction with tissues, promoting attraction and aggregation of iron containing species

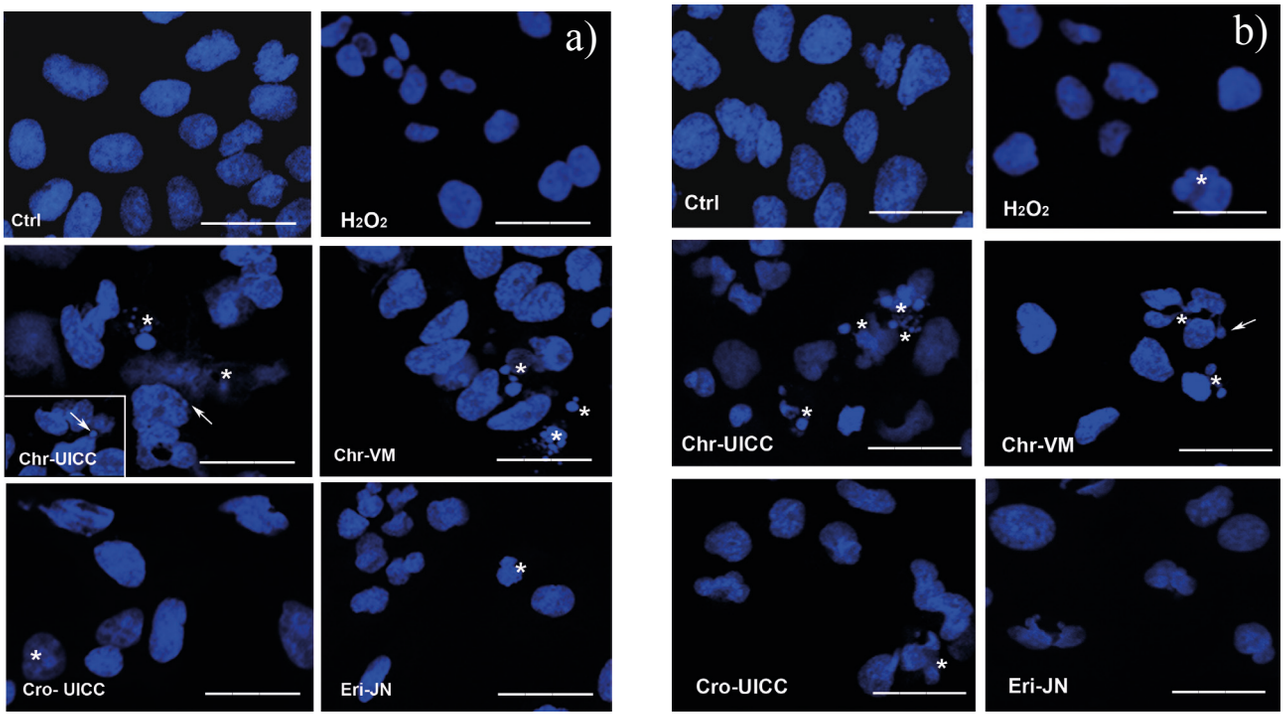

Figure 2 a,b. Fluorescent light microscopy images after DAPI assay to detect nuclear aspect of MeT5A (A) and A549 (B) cells at 24 h. In both cultures control cells showed normal fluorescent nuclei, while in treated cultures nuclear bodies (*) and micronuclei (↑) were detectable in apoptotic cells. These aspects were mostly found after fibres contacts, in particular after chrysotile treatments. 400 μM H_2O_2 treated cells were considered as positive control. Scale bars = 10 μm.

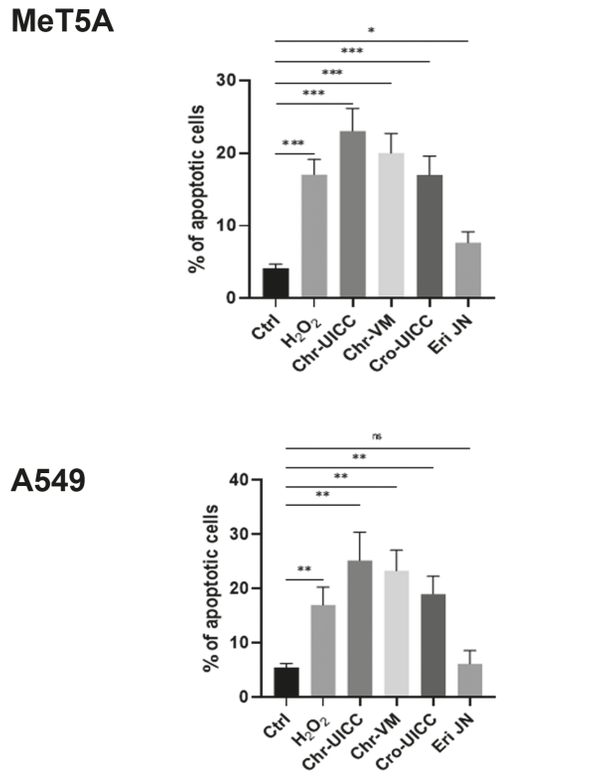

Figure 2c. Morphometrical evaluations of apoptotic cells with nuclear bodies (*) and micronuclei (↑) that were mostly found after fibres contacts.

as tissue deposition of asbestos fibres that culminate in asbestos bodies formation (Pascolo et al., 2011).

EPR Spin Trapping Results

EPR spectra are reported in Figure 4. All analysed fibres showed the immediate production of spin-adducts, and different behaviours were observed after 1h of incubation. The molar concentrations of the [DMPO-OH]• adducts are collected in Table 3. After 5 min of incubation CHR-UICC fibre resulted the most active in $HO^{\bullet}$ radicals generation, while Eri-JN was found to be the least reactive of the asbestos studied. After 1h of incubation, the most active fibre was the Cro-UICC, while the fibre least capable of generating adducts still resulted Eri-JN.

ATR-FTIR characterization

Figure 5 shows the characteristic infrared spectra of the four types of asbestos samples studied, exemplifying the key bands observed and highlighting significant differences among all types of asbestos. Two regions in the spectra are of particular interest: the 3700-3500 cm^{-1} region, attributed to O-H stretching vibrations and 1200-500 cm^{-1} region, ascribed to various lattice vibrations (Sontevska et al., 2007). FTIR spectra in both the OH-stretching region and in the lattice modes region can be effective for rapid identification of the asbestos type. In the spectra of Chr-UICC and Chr-VM two IR bands are well visible in the region 4000-3000 cm^{-1}: the first (strong) at 3684 cm^{-1} is due to the surface Mg-OH stretch vibration and the second (weaker) at 3664 cm^{-1} is linked to the inner Mg-OH stretch vibration (Fujishige et al., 2007). This confirms the assignment of the OH doublet to the external and internal Mg-OH groups in chrysotile asbestos (Jolicoeur and Duchesne, 1981). In addition, the band at ~601cm^{-1} can be assigned to the inner Mg-OH vibration (Ristic et al., 2011). The IR bands recorded in the region ~1080-935 cm^{-1}, present in all samples, are typical of the Si-O-Si stretching in the silica network. For Cro-UICC and Eri-JN, FT-IR analysis showed a major Fe and Na content (IR bands at 777-780 cm^{-1}) and the presence of some impurities, due to the presence of several small bands in the region between 800-500 cm^{-1}. The IR bands recorded in the region ~1400-1500 cm^{-1} may indicate the presence of carbonates.

Cell viability

Cell viability was evaluated through the MTT assay. As shown in Figure 6, a significant decrease in formazan

Table 1. Morphometrical evaluation of apoptotic bodies and micronuclei from DAPI stained images of MeT5A and A549 cell lines. Data are expressed as mean ± sd of % values.

MeT5A	Mean ± sd
Ctrl	2 ± 0.2
H_2O_2	15 ± 1.3
Chr-UICC	35 ± 4.5
Chr-VM	27 ± 3.2
Cro-UICC	20 ± 2.4
Eri JN	7.4 ± 1.2
A549	**Mean ± sd**
Ctrl	3.5 ± 0.5
H_2O_2	17± 3.3
Chr-ICC	37.2 ± 6.1
Chr-VM	28.3 ± 4.5
Cro-ICC	22 ± 3.5
Eri JN	6.2 ± 3.4

Statistical analysis performed comparing untreated (Ctrl) vs fibres treated cultures of MeT5A and A549 cell lines at 24. Student's t test analysis p*=<0.05; **=<0.01; ***=<0.001. (See Figure 2 a,b).

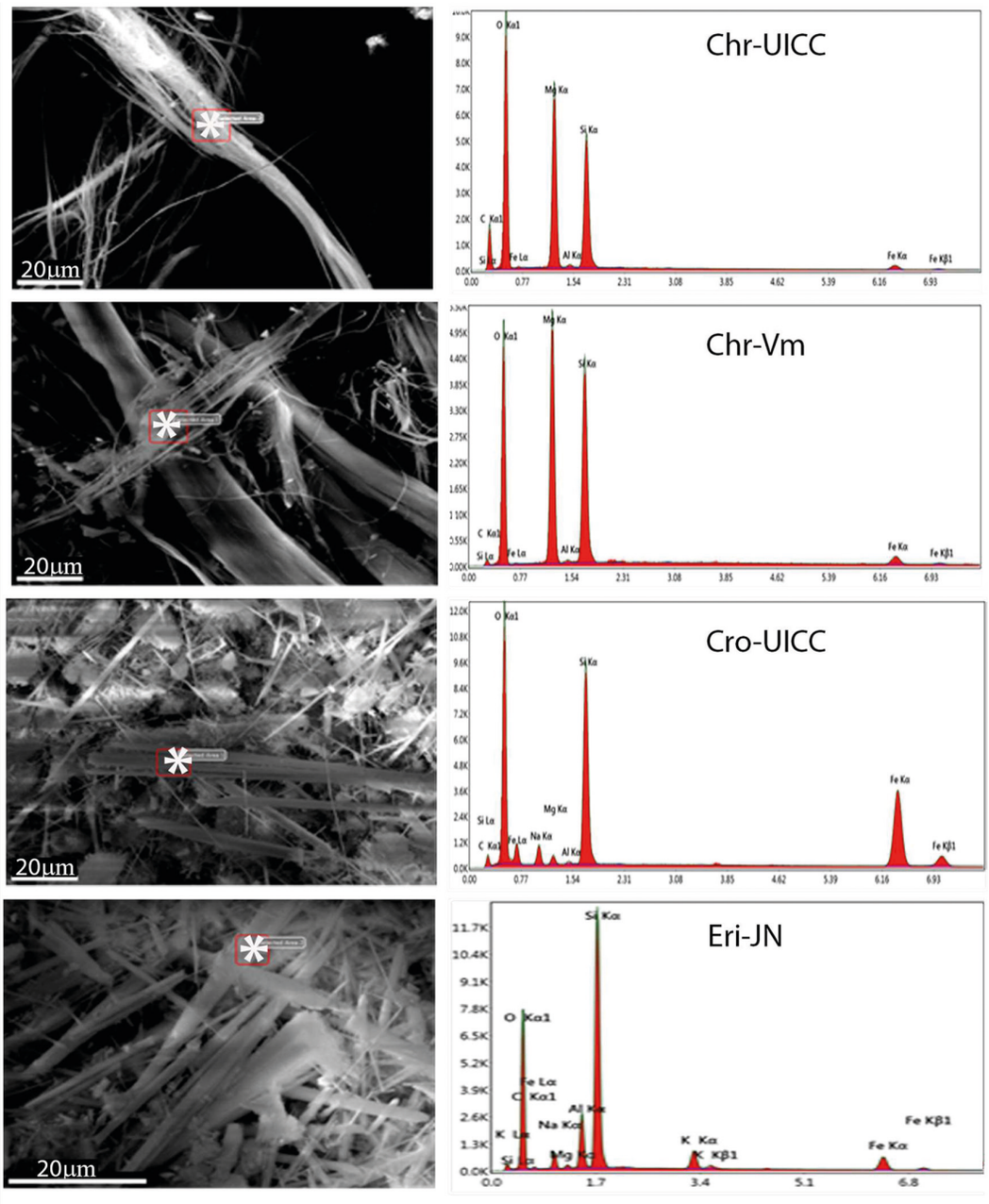

Figure 3a. SEM EDAX investigation. Second electron SEM images of the raw fibres, and relative dispersive energetic spectrum EDS-SEM performed at selected spots (*).

levels was observed in both cell lines following treatment with 50 mg/ml of the indicated fibres suspensions, with higher effects detected after 24 and 48 h ($p<0.001$). In MeT5A (Figure 6a and Table 4), Chr-UICC treatment showed a reduction in OD (reported as percentage with respect to untreated cells, referred as 100%) to 51.4%, Chr-VM to 23%, Cro-UICC to 37.3% and Eri-JN to 36.4% at 24 h; lower levels of formazan were observed at 48 h as reported in Table 3. Comparable results were observed in A549 cell cultures (Table 4).

Taking into consideration that the amount of signal generated by the MTT assay reflects mitochondrial dehydrogenase activity, and therefore the overall cellular metabolic status, we proceeded with the direct cell count by trypan blue staining (Table 5). Results showed a slight effect on cell survival particularity due to Chr-UICC treatment: after these fibres treatments, the MTT results showed mainly a reduced cellular metabolic activity rather

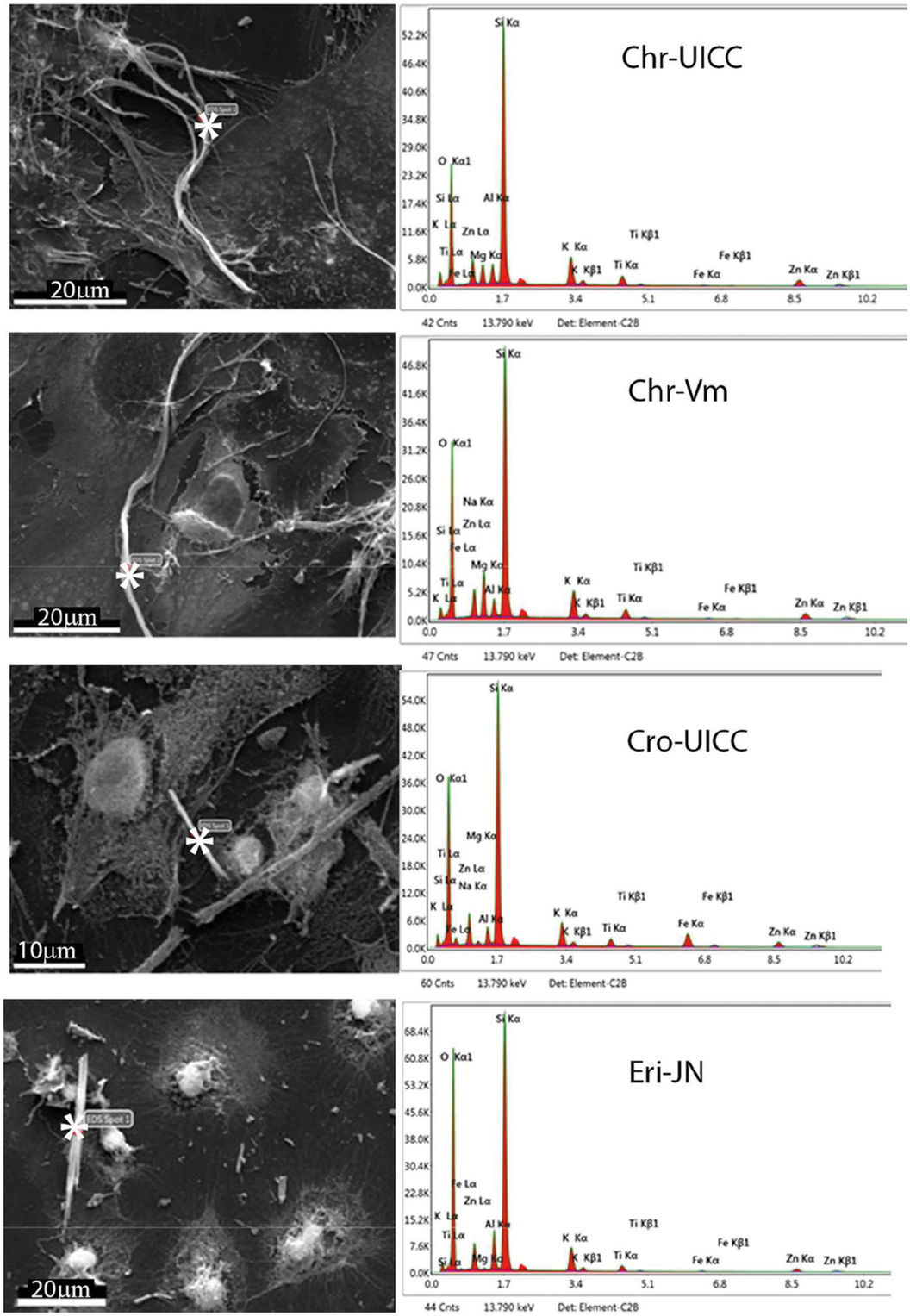

Figure 3b. SEM EDAX investigation. Fibres in MeT5A cultures, and relative dispersive energetic spectrum EDS-SEM performed at selected spots (*).

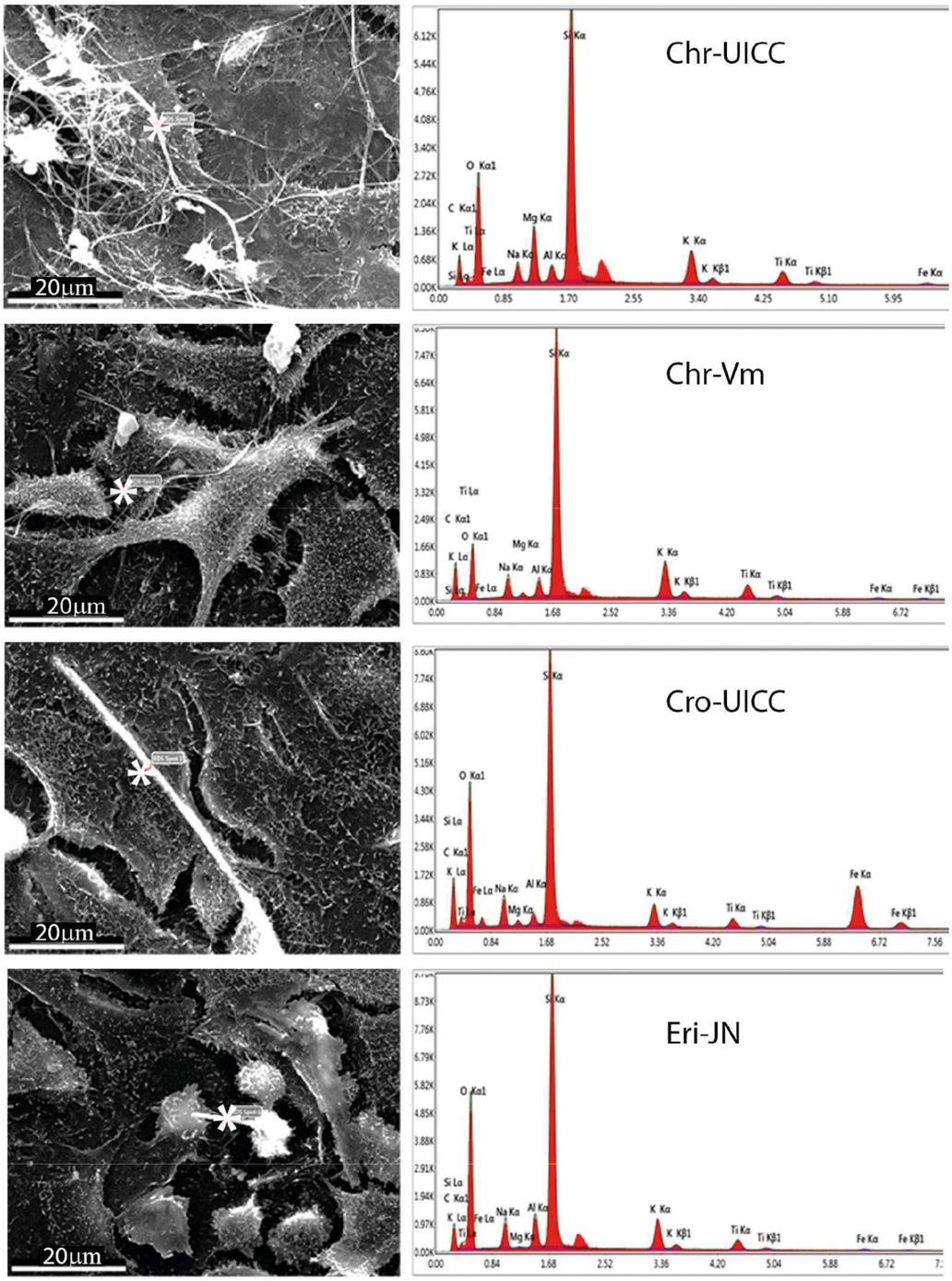

Figure 3c. SEM EDAX investigation. Fibres in A549 cultures, and relative dispersive energetic spectrum EDS-SEM performed at selected spots (*).

than a total cytotoxic effect. At 48 h (Table 5), an effect on cell survival following Chr-UICC treatment is evident. However, in both cell lines, we did not observe significant differences among untreated, Chr-VM, Cro-UICC, Eri-JN treated cells. In should be remarked that, despite the fact that MTT assay was developed for cell viability screening, results should be carefully interpreted. We said that this method measures the reduction of yellow MTT to the

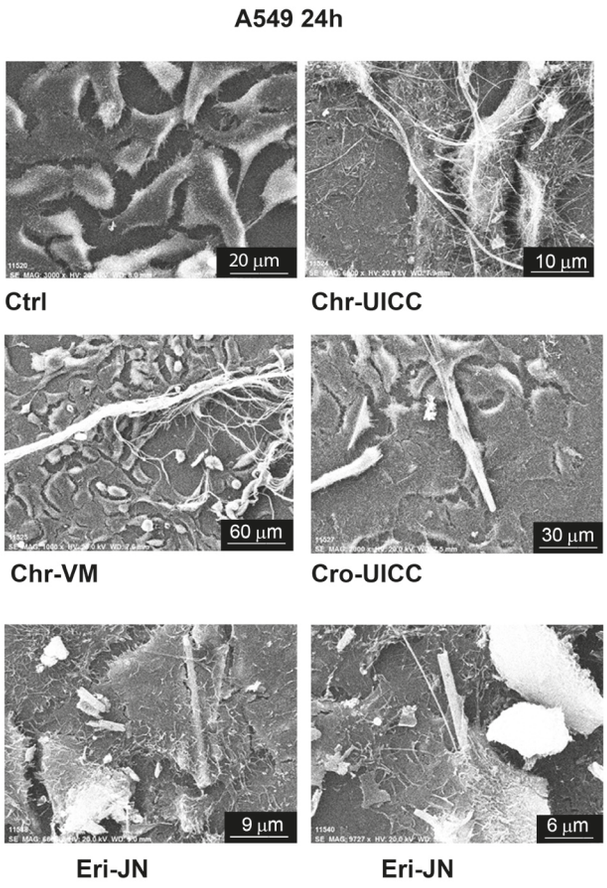

Figure 3d. Secondary electron SEM image of A549 cultured cells exposed to Chr-UICC, Chr-VM, Cro-UICC, and Eri-JN fibres. Close contacts of fibres can be detected in contact with cell surface engaged in attempt of asbestos uptake. Fibres uptake after Eri-JN treatment was more evident due to the smaller size of the fibres.

insoluble blue formazan product by mitochondrial succinate dehydrogenase (Kumar et al., 2018). The reduction in the formation of formazan crystal observed with MTT assay was not fully comparable to the results obtained after direct cell counting by trypan blue staining. Although some reduction inside viability has been observed the results obtained by colorimetric reaction could be mostly attributable to an impairment of mitochondrial function activity rather than a real cytotoxic effect.

The comparison of the biological activity of the investigated fibres shows that the MTT cell viability of Chr-VM is greater than that of the asbestos standards Chr-UICC and Cro-UICC. The cell viability of Chr-UICC is lower than that of Cro-UICC. This apparently surprising result is in line with the literature findings. In fact, Craighead et al., (1980) and Mossman et al. (2011) observed that chrysotile is more cytotoxic than crocidolite or amosite at the same mass or fibre concentration in rodent and human lung epithelial and mesothelial cells. In general, the cell viability of Eri-JN is greater than that of the other investigated fibres. At both time points, the negative carcinogenic standard wollastonite (wol) has the less cytotoxic effect (as reported in Figure 6).

ROS production

The cell viability id correlated with the intracellular ROS levels that provide information about the ordinary biologic processes inside the cells. ROS imbalance interferes with normal cell functions and, for this reason, it is considered indicative of cell damage (Damiani et al., 2018). To determine the effect of asbestos fibres on intracellular ROS generation, we measured DCF fluorescence in the presence or absence of Chr-UICC, Chr-VM, Cro-UICC or Eri-JN 50 mg/ml at different time point in both MeT5A and in A549 cell cultures. Fibres insult resulted in an increased ROS intracellular levels in both cell cultures following 6h treatment (Figure 7 a,b), with the highest values recorded at 24 h. In MeT5A cells, the increase observed was 187.1 and after Chr-UICC; Chr-VM; Cro-UICC and Eri-JN treatments respectively compared to untreated cultures (Figure 7a). In A549 cells (Figure 7b) at 24 h an increase was detected equal to 621.74 and for Chr-UICC, Chr-VM; Cro-UICC and Eri-JN respectively compared to untreated controls. It has been already established that ROS are important mediators of asbestos-induced human diseases and their correlation with fibres sustain indirect DNA damage *in vivo* via formation of 8-hydroxy-2'-deoxyguanosine (8-OHdG) adducts (Xu et al., 1999). Moreover, according to Kinnula et al. (1999) the generation of ROS by asbestos fibres appears to be variable on the basis of the characteristics of the fibres. Indeed, in Met5A and A549 cell line, the ROS analysis detected different increase of ROS levels after asbestos exposure, suggesting a correlation with fibres kind (Roney et al., 1989).

Although the data for the Met5A at 24 h appear anomalous and difficult to interpret, some general trends can be outlined. For both cell lines: the ROS production from Chr-UICC is greater or equal to that of Chr-VM and Cro-UICC; the ROS production from Chr-VM is greater or equal to that of Cro-UICC; the ROS production from Eri-NJ is lower or equal to that of all the other fibres.

Effects on glutathione content

We also decided to investigate cellular processes involved to contrast oxidative stress caused by the contact with the fibres, and especially the total GSH, one of the crucial scavengers in cells (Haenen and Bast, 2014). Glutathione is an important non-enzymatic antioxidant that responds to the redox status of the cell by reacting

Table 2. Chemical analysis obtained by SEM-EDAX.

a) original dry asbestos fibres.

Element (wt%)	Chr-UICC	Chr-VM	Cro-UICC	Eri-JN
Silicon	17.62 ± 6.1	16.77 ± 6.19	23.52 ± 5.56	29.73 ± 5.0
Aluminium	0.39 ± 0.14	0.39 ± 0.04	0.31 ± 0.06	7.55 ± 0.90
Magnesium	19.69 ± 4.49	25.06 ± 0.92	1.62 ± 0.12	0.52 ± 0.20
Iron	1.11 ± 0.41	1.54 ± 0.46	23.01 ± 3.87	4.09 ± 2.3

b) fibres added to MeT5A cultured cells at 48 h.

Element (wt%)	Chr-UICC	Chr-VM	Cro-UICC	Eri-JN
Silicon	28.92 ± 5.21*	32.9 ± 4.93**	25.44 ± 5.05	30.89 ± 4.86
Aluminium	2.8 ± 0.42****	3.01 ± 0.01****	2.68 ± 0.02***	4.87 ± 0.10***
Magnesium	5.25 ± 1.69****	2.64 ± 1.00****	0.58 ± 0.41***	0.23 ± 0.01*
Iron	0.13 ± 0.02***	0.18 ± 0.04***	4.39 ± 2.25****	0.27 ± 0.03**

c) fibres added to A549 cultured cells at 48h.

Element (wt%)	Chr-UICC	Chr-VM	Cro-UICC	Eri-JN
Silicon	22.24 ± 0.28	22.68 ± 1.02	19.17 ± 2.12	26.24 ± 4.95
Aluminium	1.72 ± 0.03****	1.91 ± 0.13****	1.35 ± 0.25****	3.05 ± 0.24****
Magnesium	6.35 ± 0.70***	0.95 ± 0.22****	0.65 ± 0.16****	0.11 ± 0.01***
Iron	0.35 ± 0.04**	0.33 ± 0.04***	4.84 ± 1.25****	0.25 ± 0.02**

d) cell culture support glass.

Element (wt%)	
Silicon	22.53 ± 0.99
Aluminium	2.59 ± 0.06
Magnesium	0.00 ± 0.00
Iron	0.00 ± 0.00

Statistical analysis performed by comparing weight % of fibres minerals expressed as mean values ± SD of: a) original dry asbestos fibres vs b) fibres added to MeT5A cultures at 48 h and c) fibres added to A549 cultures at 48 h. Student's t test: p*=<0.05; **=<0.01; ***=<0.001; ****=<0.0001.

directly with ROS; therefore, its levels were also evaluated in both cell cultures following asbestos fibres treatment at different time point. In our study, the total intracellular glutathione content resulted globally decreased in all treated cultures (Figure 8), with respect to the control values. Slight decrements of levels ($p<0.05$) were evident since 6 h in MeT5A cells after Chr-UICC treatment (Figure 8a). At 24 and 48 h glutathione contents were affected also by Cro-UICC and Eri-JN fibres, with higher loss of function exerted by Chr-UICC fibres ($p<0.001$).

Higher significant depletions ($p<0.001$) were observed in A549 cultures at all time points, since short time of treatments (Figure 8B). Higher grade of loss in glutathione contents were observed with Chr-UICC at all time points. Chr-VM and Eri-JN fibres also affected antioxidant levels in a significant way with stronger decrements compared to Cro-UICC and control values.

Even for this assay, the data for the Met5A at 24 h appear anomalous. Notwithstanding, general trends inversely correlated with ROS production can be outlined from Figure 7. For both cell lines: glutathione depletion induced by Chr-UICC is greater than that of all the other fibres; glutathione depletion by Chr-VM is greater than that of Cro-UICC; glutathione depletion by Eri-NJ is lower or

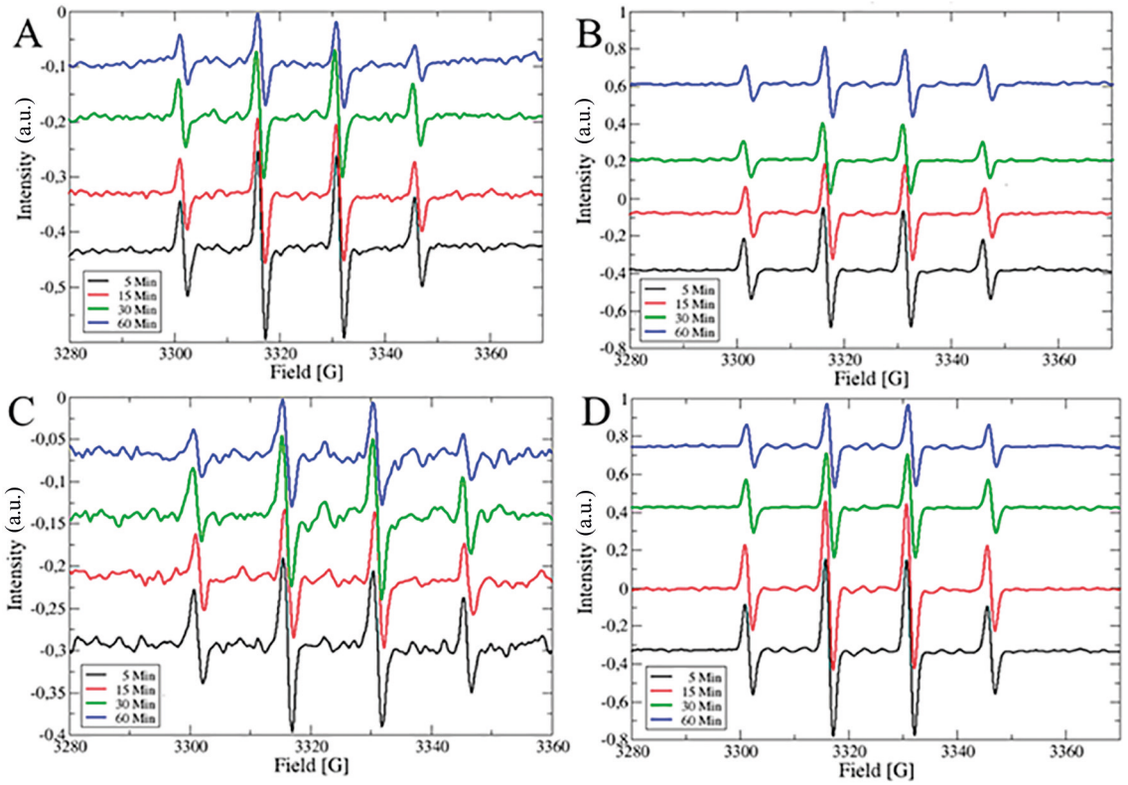

Figure 4. EPR spectra of [DMPO-OH]• adduct obtained from (A) Chr-UICC, (B) Chr-VM, (C) Cro-UICC, and (D) Eri-JN fibres.

Table 3. Molar concentration of [DMPO-HO]• adduct in each asbestos sample.

Time (min)	CHR-UICC	CHR-VM	Cro-UICC	Eri-JN
5	8,00 x 10^{-6} M	3,66 x 10^{-6} M	2,76 x 10^{-6} M	1,87 x 10^{-6} M
15	2,76 x 10^{-6} M	3,41 x 10^{-6} M	2,52 x 10^{-6} M	1,30 x 10^{-6} M
30	1,48 x 10^{-6} M	2,52 x 10^{-6} M	2,17 x 10^{-6} M	5,74 x 10^{-7} M
60	1,11 x 10^{-6} M	1,85 x 10^{-6} M	1,90 x 10^{-6} M	3,29 x 10^{-7} M

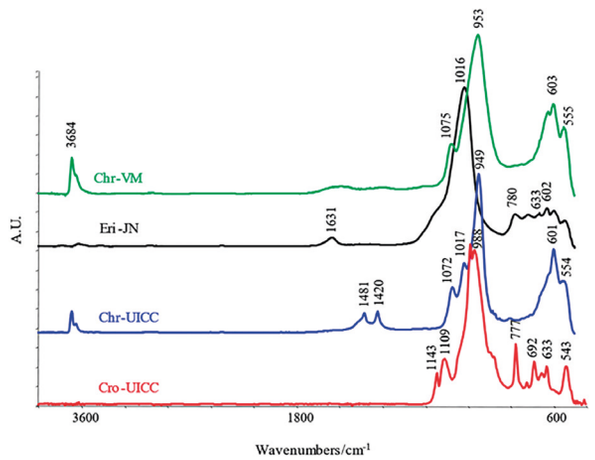

Figure 5 a,b,c,d. FTIR average spectra of the studied asbestos fibres: two different natural non-commercial asbestos fibres, Chr-VM and Eri-JN fibres compared to standard asbestiform minerals, UICC chrysotile (Chr-UICC) and UICC crocidolite (Cro-UICC).

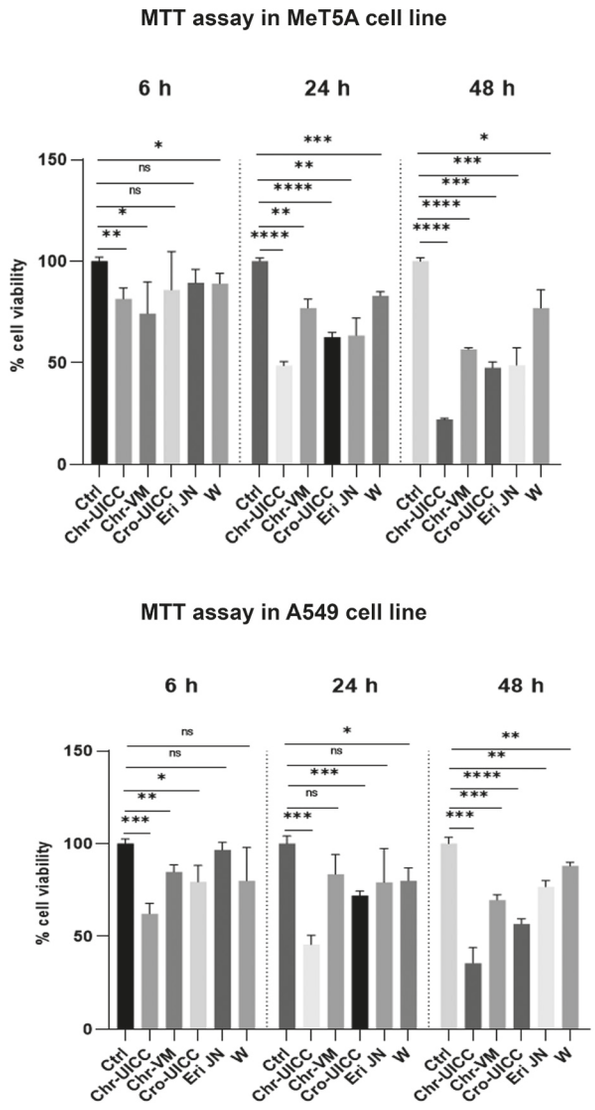

Figure 6. MTT assay on MeT5A and A549 cells in absence (CTRL) or after exposure to asbestos fibres (50 µg/ml) solution of Chr-UICC, Chr-VM, Cro-UICC, Eri-JN and Wollastonite fibres at 6, 24 and 48 h. Wollastonite fibres were considered as standard negative controls. Data are normalized to CTRL and reported as mean ± sd. with p values equal to: * $p<0.05$, ** $p<0.01$, *** $p<0.001$, **** $p<0.0001$.

equal to that of all the other fibres with the anomaly of the A549 tests at 24 h and 48 h where a depletion is actually observed.

Interpretation of the observed differences in the fibre-cell interaction

Here, the cytotoxicity *in vitro* of the investigated naturally occurring chrysotile and fibrous erionite fibres has been confirmed. There are differences with respect to the prediction of the toxicity/pathogenicity potential delivered by the Fibre Potential Toxicity Index (FPTI) (Gualtieri, 2018). In that model, the calculated FPTI values of UICC crocidolite, Jersey erionite-Na, UICC chrysotile and Valmalenco chrysotile were 2.67, 2.35, 2.18 and 2.14, respectively. Qualitatively, the FPTI rank is Valmalenco chrysotile<UICC chrysotile< Jersey erionite-Na<UICC crocidolite. This predictive model is a theoretical tool to predicting the potential toxicity and carcinogenicity of a mineral fibre based on all its crystal-chemical-physical parameters inducing biological adverse effects. These effects determine the cyto-toxicity and geno-toxicity *in vitro* (acute effects in cell cultures), cyto-toxicity and geno-toxicity *in vivo* (acute and medium-term effects in animal studies, namely rats), and carcinogenicity *in vivo* (long term-chronic effects in animals and human epidemiological studies). The results of this study deal only with cyto-toxicity *in vitro* measured in mesothelial Met5A and epithelial A549 cell cultures. Hence, they capture a partial picture of the scenario, focussed on the acute effects (≤48 h) induced by the fibres on the cells. It should also be remarked that the cell types used in this study are not specialized in the phagocytosis clearance action like macrophages, but can display sporadic phagocytic and engulfment activity, as already reported for A549 (Cavallo et al., 2004; Pugnaloni et al., 2015). Said that, the drawn qualitative rank for the cell viability is Jersey erionite-Na>Valmalenco chrysotile>UICC crocidolite>UICC chrysotile. Symmetrically, the qualitative rank for the ROS production is Jersey erionite-Na<Valmalenco chrysotile»UICC crocidolite<UICC chrysotile.

The chemical composition is strictly correlated to the ability of the asbestos fibres to generate a damage. To better evaluate the intrinsic reactivity of each species, the formation of $HO^{\bullet}$ radicals was monitored in vitro, by means of the EPR-Spin Trapping technique. In fact, the release of the hydroxyl radical in the presence of H_2O_2 is held to occur *in vivo* when asbestos fibres are exposed to lysosomal fluids during alveolar macrophage phagocytosis (given that the role of neutrophils in this sense could be very important), promoting a direct oxidative stress. EPR analysis showed that all studied fibres generated different amounts of [DMPO-OH]• adduct. This means that all the four asbestoses studied had Fe ions on their surfaces; in addition, the differences in the EPR spectra intensities must be ascribed to different amount of released Fe^{2+} between different fibres. In fact, during the 1 h detection, Eri-JN samples showed the less intense EPR spectra because its (known) less concentration of iron on the surface with respect to the other fibres under investigation. Conversely, Cro-UICC showed the most intense EPR

Table 4. Cell viability assay obtained by MTT test investigations in control and treated MeT5A and A549 cells at 6, 24 and 48 h. Untreated control cells were considered as 100% of cell viability. % mean values ± sd.

a) MeT5A

MTT test	6h	24h	48h
% values X ± SD			
1 CTRL	100 ± 2.12	100 ± 1.62	100 ± 1.81
2 Chr-UICC	81.60± 5.27	48.57± 2.11	22.23 ± 0.58
3 Chr-VM	74.34 ± 15.63	76.98 ± 4.46	56.71 ± 0.92
4 Cro-UICC	85.96 ± 18.77	62.67 ± 2.29	47.66 ± 2.86
5 Eri-JN	89.43 ± 6.72	63.62 ± 8.47	48.91 ± 8.54
6 W	89 ± 5	83 ± 2	77 ± 9

b) A549

MTT test	6h	24h	48h
% values X ± SD			
1 CTRL	100 ± 2.51	100 ± 4.23	100 ± 3.51
2 Chr-UICC	62.31 ± 5.59	45.67 ± 5.01	38.99 ± 12.85
3 Chr-VM	84.78 ± 3.85	83.60 ± 10.63	69.66 ± 2.88
4 Cro-UICC	79.41 ± 8.85	71.98 ± 2.51	56.77 ± 2.80
5 Eri-JN	96.38 ± 3.73	79.22 ± 18.29	76.81 ± 3.44
6 W	80 ± 18	80 ± 7	88 ± 2

Statistical analysis performed comparing untreated (CTRL) vs fibres treated cultures of MeT5A (a) and A549 cell lines (b) at 6, 24 and 48 h. Student's t test analysis p* =<0.05; ** =<0.01; *** =<0.001. (See fig. 5)

Table 5. Cell viability assay obtained by trypan blue exclusion test in MeT5A and A549 cultures at 48 h. % mean values ± sd.

Cell type	CTRL	Chr-UICC	Chr-VM	Cro-UICC	Eri-JN
MeT5A	17.10 ± 4.94	22.50 ± 3.53	28.45 ± 2.19	20.31 ± 14.2	20.2 ± 0.14
A549	11.15 ± 2.05	39.75 ± 1.76**	9.10 ± 0.56	12.85 ± 1.06	19.4 ± 5.09

Statistical analysis performed comparing: CTRL (untreated cells) vs fibres added to MeT5A and A549 at 48 h. Student's t test analysis ** = p<0.01.

spectra after 1 h of incubation, evidencing the already described high amount of surface Fe ions. Very interesting is the differences found between Chr-UICC and Chr-VM: the total amount of adduct for the first moved from $8 \cdot 10^{-6}$ to $1.11 \cdot 10^{-6}$ M, resulting the most active at the beginning of the experiment, showing a drastic $HO^{\bullet}$ concentration decrease after the first 15 min. On the other hand, the [DMPO-OH]• adduct concentration for Chr-VM moved from 3.66×10^{-6} M (after 5 min) to 1.85×10^{-6} M (after 1 h), but final slightly higher concentrations with respect to those observed for Chr-UICC. These different behaviours seem in line with the responses from MTT cell viability experiments, where a larger toxicity of Chr-UICC with respect to Chr-VM has been found in both cell lines used, attributed to a higher content of Fe^{2+} in the first asbestos. On the other hand, the slower [DMPO-OH]• adduct concentration decrease found for Chr-VM likely indicates a slower release of Fe^{2+} with time in this kind of asbestos.

Fourier Transform Infrared spectroscopy (FTIR) also represents a valuable tool for the identification and crystal-chemical study of fibrous minerals, and asbestos amphiboles in particular. As observed by EDAX and EPR investigations, samples of Chrysotile groups (Chr-UICC and VM) and Cro-UICC and Eri-JN ones showed

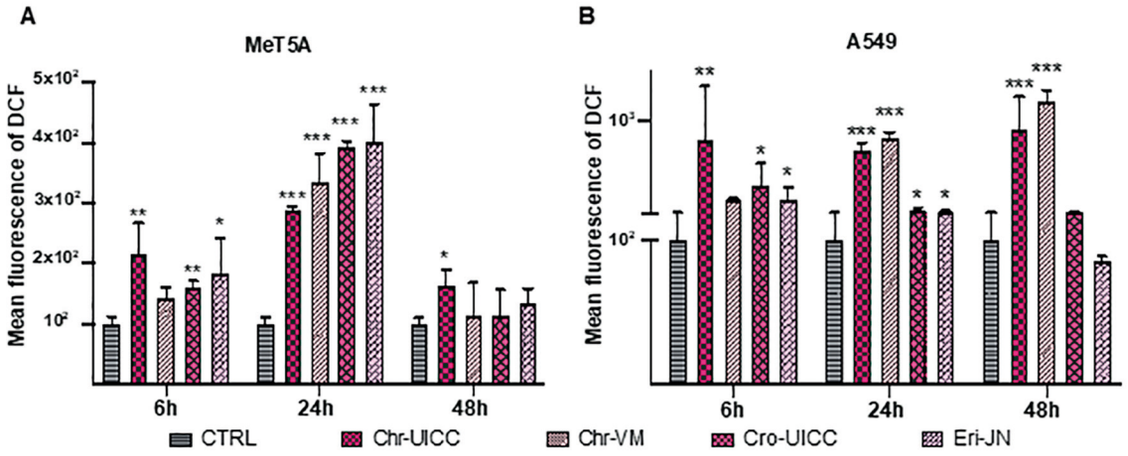

Figure 7 a,b. Evaluation of ROS production in MeT5A (a) and A549 (b) by flow cytometry analysis following treatment of Chr-UICC, Chr-VM, Cro-UICC and Eri-JN at 6, 24 and 48 h. Data are reported as mean fluorescence intensity in % related to control (untreated cells). Values represent mean ± sd of at least three independent experiments. * =p<0.05; ** = p<0.01; *** =p<0.001.

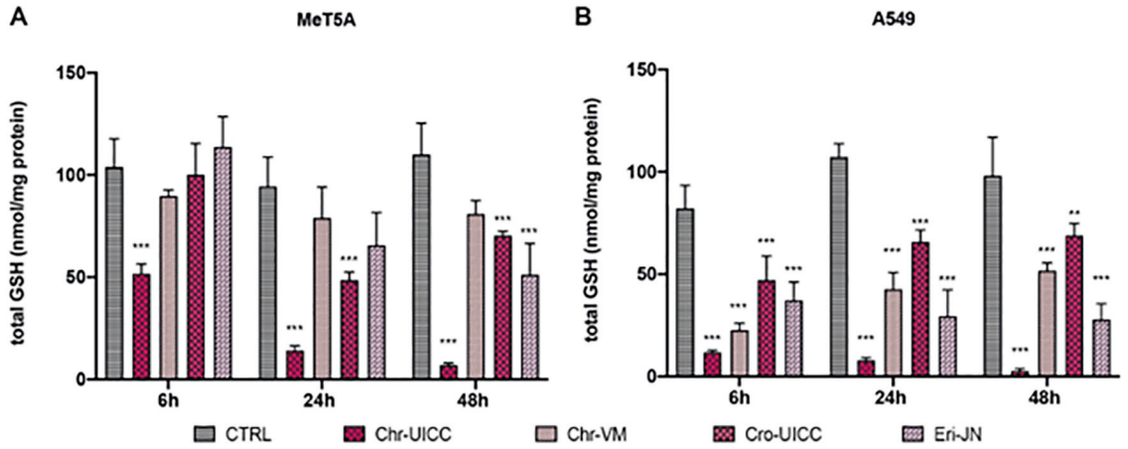

Figure 8 a,b. Levels of total intracellular glutathione analysed on MeT5A (a) and A549 (b) showing a significant depletion of total glutathione respect the untreated cells (CTRL). Data reported as mean ± sd. **p<0 .01; ***p<0 .001 and compared to CTRL.

a different composition, being the former richer in Mg while the latter in Fe ions, as well as containing some iron-rich impurities. These differences are crucial for evaluating the biological effects of asbestos fibres on cell cultures, also correlated to the production of [DMPO-OH]• adduct. In order to evaluate a possible connection between fibre-associated superficial elements loss, free radical activity and glutathione pathway, we considered important to evaluate the superficial iron and magnesium release from fibres in cultures, considered as element loss from the native mineral.

In agreement with past literature data (see for example, Craighead et al., 1980; Mossman et al., 2011) showing that chrysotile is more cytotoxic than crocidolite in human lung epithelial and mesothelial cells, we have seen that Chr-UICC is more cytotoxic and promotes greater ROS production than the other standard Cro-UICC in the investigated cell cultures within the time span 0-48h. The greater acute toxic insult of chrysotile with respect to crocidolite can be explained by the so-called 'Trojan Horse Effect' (Gualtieri et al., 2019) for which, chrysotile when phagocytosed, undergoes fast dissolution upon contact with intracellular acidic fluids. Dissolution of the octahedral sheet of the chrysotile fibres results in a release of metals like iron with cytotoxic action. This occurs to a much lesser extent for biodurable crocidolite, which therefore exerts less acute toxicity insults. The qualitative trend of decrease of Mg and Fe content detected in the

chrysotile fibres in cultures with respect to the pristine cases (Figure 2) support this model.

Although it is cytotoxic, we have seen that erionite Eri-JN displays a greater cell viability and lower ROS production in the investigated cell systems in the time span 0-48h. The results are in line with the observations made to test the acute effects of mineral fibres *in vitro* using phagocytic THP-1 cells by Di Giuseppe et al. (2022) in the 0-8 h time span and Mirata et al. (2022) in the 0-24 h time span. Erionite fibres are able to induce an intracellular ROS increase but its contribution is lower than both crocidolite and chrysotile stimuli. Because the erionite fibres are short in length, frustrated phagocytosis by THP-1 cells plays a limited role in the acute toxicity of this fibre.

CONCLUSIONS

The cytotoxicity *in vitro* of naturally occurring chrysotile and fibrous erionite fibres has been confirmed by our systematic study.

The cell viability of Jersey erionite-Na is greater than that of Valmalenco chrysotile which is, in turn, greater than that of the asbestos standards UICC crocidolite and UICC chrysotile. Because cytotoxicity is related to the production of ROS, the latter is in line with the cell viability data: Jersey erionite-Na<Valmalenco chrysotile»UICC crocidolite<UICC chrysotile.

Further studies will be required to better elucidate the mechanisms engaged by such asbestos fibres from natural outcrops. In particular, other investigations are going to support the present study examining the DNA damage with the Comet assay and the phosphorylation rate of g-H2A.X histone to highlight the genotoxic character and deeper analyse the peculiar pathways activated during the DNA damage mechanisms and DNA repair potential by RAD51, a protein involved in repair of damage associated with DNA replication in mammalian cells.

ACKNOWLEDGEMENTS

This work is the outcome of a long-term research projects “Fondi di Ateneo per la Ricerca (FAR 2017) - Fibre potential toxicity Index (FPTI)” and “PROGETTI DI RICERCA DI RILEVANTE INTERESSE NAZIONALE - PRIN Bando 2017 - Prot. 20173X8WA4 - Fibers A Multidisciplinary Mineralogical, Crystal-Chemical and Biological Project to Amend the Paradigm of Toxicity and Cancerogenicity of Mineral Fibers”.

Adriano Di Cristoforo (CISMIN, Università Politecnica delle Marche) is sincerely acknowledged for SEM-EDAX support and fruitful discussions.

REFERENCES

Ballirano P., Bloise A., Gualtieri A.F., Lezzerini M., Pacella A., Perchiazzi N., Dogan M., Dogan A.U., 2017. The crystal structure of mineral fibres. In: Mineral fibres: crystal chemistry, chemical-physical properties, biological interaction and toxicity 18, 17-53.

Ballirano P. and Cametti G., 2015. Crystal chemical and structural modifications of erionite fibers leached with simulated lung fluids. American Mineralogist 100, 1003-1012.

Bloise A., Barca D., Gualtieri A.F., Pollastri S., Belluso E., 2016. Trace elements in hazardous mineral fibres. Environmental Pollution 216, 314-323.

Baumann F., Buck B.J., Metcalf R.V., McLaurin B.T., Merkler D.J., Carbone M., 2015. The Presence of Asbestos in the Natural Environment is Likely Related to Mesothelioma in Young Individuals and Women from Southern Nevada. Journal of Thoracic Oncology 10, 731-737.

Bernstein D.M., 2014. The health risk of chrysotile asbestos. Current Opinion on Pulmonary Medicine 20, 366-70.

Bloise A., Barca D., Gualtieri A.F., Pollastri S., Belluso E., 2016. Trace elements in hazardous mineral fibres. Environmental Pollution 216, 314-323.

Bode B.E., Murphy D.M., Chechik V. (Eds.), 2020. Electron Paramagnetic Resonance: Volume 27, Royal Society of Chemistry.

Brigelius R., Muckel C., Akerboom T.P., Sies H., 1983. Identification and quantitation of glutathione in hepatic protein mixed disulfides and its relationship to glutathione disulfide. Biochemical pharmacology 32, 2529-2534.

Buettner G.R., 1987. Spin trapping: ESR parameters of spin adducts. Free Radical Biology and Medicine 3, 259-303.

Bursi Gandolfi N., Gualtieri A.F., Pollastri S., Tibaldi E., Belpoggi F., 2016. Assessment of asbestos body formation by high resolution FEG-SEM after exposure of Sprague-Dawley rats to chrysotile, crocidolite, or erionite. Journal of hazardous materials 306, 95-104.

Carbone M., Emri S., Dogan A.U., Steele I., Tuncer M., Pass H.I., Baris Y.I., 2007. A mesothelioma epidemic in Cappadocia: scientific developments and unexpected social outcomes. Nature Reviews Cancer 7, 147-154.

Carbone M. and Yang H., 2017. Mesothelioma: recent highlights. Annals of Translational Medicine 5(11), 238-244.

Cattaneo A., Somigliana A., Gemmi M., Bernabeo F., Savoca D., Cavallo D.M., Bertazzi P.A., 2012. Airborne concentrations of chrysotile asbestos in serpentine quarries and stone processing facilities in Valmalenco, Italy. Annals of occupational hygiene 56, 671-683.

Cavallo D., Campopiano A., Cardinali G., Casciardi S., De Simone P., Kovacs D., Perniconi B., Spagnoli G., Ursini C.L., Fanizza C., 2004. Cytotoxic and oxidative effects induced by man-made vitreous fibers (MMVFs) in a human mesothelial cell line. Toxicology 201, 219-229.

Chalfont G.R., Perkins M.J., Horsfield A., 1968. Probe for homolytic reactions in solution. II. Polymerization of styrene. Journal of the American Chemical Society 90, 7141-7142.

Comba P., Merler E., Pasetto R., 2005. Asbestos-related diseases

in Italy: epidemiologic evidences and public health issues. International Journal of Occupational and Environmental Health 11, 36-44.

Craighead J.E., Mossman B.T., Ezerman E.B., Adler K.B., 1980. Isolation and spontaneous trans-formation of hamster tracheal epithelial cells. Cancer Research 40, 4403-4409.

Damiani E., Brugè F., Cirilli I., Marcheggiani F., Olivieri F., Armeni T., Cianfruglia L., Giuliani A., Orlando P., Tiano L., 2018. Modulation of oxidative status by normoxia and hypoxia on cultures of human dermal fibroblasts: how does it affect cell aging? Oxidative Medicine and Cellular Longevity, 1-16.

Di Giuseppe D., Scognamiglio V., Malferrari D., Nodari L., Pasquali L., Lassinantti Gualtieri M., Scarfì S., Mirata S., Tessari U., Hanuskova M., Gualtieri A.F., 2021b. Characterization of Fibrous Wollastonite NYAD G in View of Its Use as Negative Standard for In Vitro Toxicity Tests. Minerals 11, 1378.

Di Giuseppe D., Scarfì S., Alessandrini A., Bassi A.M., Mirata S., Almonti V., Ragazzini G., Mescola A., Filaferro M., Avallone R., Vitale G., Scognamiglio V., Gualtieri A.F., 2022. Acute cytotoxicity of mineral fibres observed by time-lapse video microscopy. Toxicology 466, 153081.

Dumortier P., Rey F., Viallat J.R., Broucke I., Boutin C., De Vuyst P., 2002. Chrysotile and tremolite asbestos fibres in the lungs and parietal pleura of Corsican goats. Occupational and environmental medicine 59, 643-646.

Franzblau A., Demond A.H., Sayler S.K., D'Arcy H., Neitzel R.L., 2020. Asbestos-containing materials in abandoned residential dwellings in Detroit. Science of the Total Environment 714, 136580.

Fubini B., Mollo L., Giamello E., 1995. Free radical generation at the solid/liquid interface in iron containing minerals. Free Radical Research 23, 593-614.

Fujishige M., Kuribara A., Karasawa I., Kojima A., 2007. Low-temperature pyrolysis of crocidolite and amosite using calcium salts as a flux. Journal of Ceramic Society of Japan 115, 434-439.

Furuya S., Chimed-Ochir O., Takahashi K., David A., Takala J., 2018. Global asbestos disaster. International Journal of Environmental research and Public Health 15, 1000.

Ghio A.J., Churg A., Roggli V.L., 2004. Ferruginous bodies: implications in the mechanism of fiber and particle toxicity. Toxicologic Pathology 32, 643-649.

Gianfagna A., Ballirano P., Bellatreccia F., Bruni B., Paoletti L., Oberti R., 2003. Characterization of amphibole fibres linked to mesothelioma in the area of Biancavilla, Eastern Sicily, Italy. Mineralogical Magazine 67, 1221-1229.

Giantomassi F., Gualtieri A.F., Santarelli L., Tomasetti M., Lusvardi G., Lucarini G., Governa M., Pugnaloni A., 2010. Biological effects and comparative cytotoxicity of thermal transformed asbestos-containing materials in a human alveolar epithelial cell line. Toxicol In Vitro. 24, 1521-31.

Giordani M., Mattioli M., Cangiotti M., Fattori A., Ottaviani M.F., Betti M., Ballirano P., Pacella A., Di Giuseppe D., Scognamiglio V., Hanuskova M., Gualtieri A.F., 2022. Characterisation of potentially toxic natural fibrous zeolites by means of electron paramagnetic resonance spectroscopy and morphological-mineralogical studies. Chemosphere 291, 133067.

Gualtieri A.F., 2018. Towards a quantitative model to predict the toxicity/pathogenicity potential of mineral fibers. Toxicology and Applied Pharmacology 361, 89-98.

Gualtieri A.F., 2023. Journey to the Centre of the Lung. The Perspective of a Mineralogist on the Carcinogenic Effects of Mineral Fibres in the Lungs. Journal of Hazardous Materials, 442, 130077.

Gualtieri A.F., Bursi Gandolfi N., Pollastri S., Pollok K., Langenhorst F., 2016. Where is iron in erionite? A multidisciplinary study on fibrous erionite-Na from Jersey (Nevada, USA). Scientific reports 6, 1-11.

Gualtieri A.F., Lusvardi G., Zoboli A., Di Giuseppe D., Lassinantti Gualtieri M., 2019. Biodurability and release of metals during the dissolution of chrysotile, crocidolite and fibrous erionite. Environmental research 171, 550-557.

Haenen G.R. and Bast A., 2014. Glutathione revisited: a better scavenger than previously thought. Frontiers in Pharmacology 5, 260-264.

Janzen E.G. and Blackburn B.J., 1968. Detection and identification of short-lived free radicals by an electron spin resonance trapping technique. Journal of the American Chemical Society 90, 5909-5910.

Jarvholm B. and Astrom E., 2014. The risk of lung cancer after cessation of asbestos exposure in construction workers using pleural malignant mesothelioma as a marker of exposure. Journal of Occupational and Environmental Medicine 56, 1297-1301.

Jolicoeur C. and Duchesne D., 1981. Infrared and thermogravimetric studies of the thermal degradation of chrysotile asbestos fibers: evidence for matrix effects. Canadian Journal of Chemistry 59, 1521-152.

Kinnula V.L., 1999. Oxidant and antioxidant mechanisms of lung disease caused by asbestos fibres. European Respiratory Journal 14, 706-716.

Klebe S., Leigh J., Henderson D.W., Nurminen M., 2020. Asbestos, smoking and lung cancer: an update. International Journal of Environmental research and Public Health 17, 258-271.

Kumar P., Nagarajan A., Uchil P.D., 2018. Analysis of cell viability by the MTT assay. Cold spring harbor protocols pdb-prot095505.

Lanone S., Rogerieux F., Geys J., Dupont A., Maillot-Marechal E., Boczkowski J., Lacroix G., Hoet P., 2009. Comparative toxicity of 24 manufactured nanoparticles in human alveolar epithelial and macrophage cell lines. Particle and Fibre Toxicology 6, 11-2.

Lagercrantz C. and Forshult S., 1968. Trapping of free radicals formed by γ-irradiation of organic compounds. Nature 218, 1247-1248.

Mirata S., Almonti V., Di Giuseppe D., Fornasini L., Raneri S., Vernazza S., Bersani D., Gualtieri A.F., Bassi A.M., Scarfì S., 2022. The Acute Toxicity of Mineral Fibres: A Systematic *In Vitro* Study Using Different THP-1 Macrophage Phenotypes. International journal of molecular sciences 23(5), 1-33.

Mossman B.T., Lippmann M., Hesterberg T.W., Kelsey K.T., Barchowsky A., Bonner J.C., 2011. Pulmonary endpoints (lung carcinomas and asbestosis) following inhalation exposure to asbestos. Journal of Toxicology and Environmental Health, Part B 14, 76-121.

Pascolo L., Gianoncelli A., Kaulich B., Rizzardi C., Schneider M., Bottin C., Polentarutti M., Kiskinova M., Longoni A., Melato M., 2011. Synchrotron soft X-ray imaging and fluorescence microscopy reveal novel features of asbestos body morphology and composition in human lung tissues. Particle and Fibre Toxicology 8, 1-11.

Pollastri S., D'Acapito F., Trapananti A., Colantoni I., Andreozzi G.B., Gualtieri A.F., 2015. The chemical environment of iron in mineral fibres. A combined X-ray absorption and Mössbauer spectroscopic study. Journal of Hazardous Materials 298, 282-293.

Pollastri S., Gualtieri A.F., Gualtieri Lassinantti M., Hanuskova M., Cavallo A., Gaudino G., 2014. The zeta potential of mineral fibres. Journal of Hazardous Materials 276, 469-479.

Pollastri S., Perchiazzi N., Lezzerini M., Plaisier J.R., Cavallo A., Dalconi M.C., Bursi Gandolfi N., Gualtieri A.F., 2016. The crystal structure of mineral fibres. 1. Chrysotile. Periodico di Mineralogia 85, 249-259.

Pugnaloni A., Lucarini G., Rubini C., Smorlesi A., Tomasetti M., Strafella E., Armeni T., Gualtieri A.F., 2015. Raw and thermally treated cement asbestos exerts different cytotoxicity effects on A549 cells in vitro. Acta Histochemica 117, 29-39.

Ristic M., Czako-Nagy I., Music S., Vertes A., 2011. Spectroscopic characterization of chrysotile asbestos from different regions. Journal of Molecular Structure 993, 120-126.

Roney P.L. and Holian A., 1989. Possible mechanism of chrysotile asbestos-stimulated superoxide anion production in guinea pig alveolar macrophages. Toxicology and Applied Pharmacology 100, 132-44.

Šontevska V., Jovanovski G., Makreski P., 2007. Minerals from Macedonia. Part XIX. Vibrational spectroscopy as identificational tool for some sheet silicate minerals. Journal of Molecular Structure 834, 318-327.

Srivastava R.K., Lohani M., Pant A.B., Rahman Q., 2010. Cyto-genotoxicity of amphibole asbestos fibers in cultured human lung epithelial cell line: role of surface iron. Toxicology and Industrial Health 26, 575-582.

Sporn T.A., 2011. Mineralogy of asbestos. Recent Results in Cancer Research 189, 1-11.

Stipa P., 2021. Recent contributions of EPR to nitrone and nitroxide chemistry. Electron paramagnetic resonance 27, 109-145.

Takahashi K. and Landrigan P.J. on behalf of the Collegium Ramazzini, 2016. Dimensions of Asbestos and Asbestos-Related Diseases. Annals of Global Health 82, 209-213.

Totaro M., Giorgi S., Filippetti E., Gallo A., Frendo L., Privitera G., Baggiani A., 2019. Asbestos in drinking water and hazards to human health: a narrative synthesis. Igiene e Sanità Pubblica 75, 303-312.

Thompson J.K., Westbom C.M., MacPherson M.B., Mossman B.T., Heintz N.H., Spiess P., Shukla A., 2014. Asbestos modulates thioredoxin-thioredoxin interacting protein interaction to regulate inflammasome activation. Particle and Fibre Toxicology 11, 1-1.

Turci F., Colonna M., Tomatis M., Mantegna S., Cravotto G., Gulino G., Aldieri E., Ghigo D., Fubini B., 2012. Surface reactivity and cell responses to chrysotile asbestos nanofibers. Chemical Research in Toxicology 25, 884-894.

Whysner J., Covello V.T., Kuschner M., Rifkind A.B., Rozman K.K., Trichopoulos D., Williams G.M., 1994. Asbestos in the air of public buildings: a public health risk? Preventive Medicine 23, 119-125.

Xu A., Wu L.J., Santella R.M., Hei T.K., 1999. Role of oxyradicals in mutagenicity and DNA damage induced by crocidolite asbestos in mammalian cells. Cancer research 59, 5922-5926.